larger than 1, implying that these gates can be used to switch subsequent stages in more complex logic circuits. Higher gains of 5 to 7 have been obtained by increasing the load resistance.

Inkjet-printed inverters can be switched at frequencies up to a few hundred hertz, as shown in Fig. 4C for the resistor-load device of Fig. 4B. The fall time $\tau_{1\rightarrow0} = 350$ μs is determined by the on current of the input transistor and by the load capacitance of our measurement setup ($C_L \approx 20$ pF). The rise time $\tau_{1\rightarrow0} = 750$ μs was designed to be comparable to the fall time by adjusting the load resistance ($R_L = 47$ megohm). We estimate the total power consumption of an inverter stage, as in Fig. 4B, to be about 2 μW when switching five subsequent inverter stages (fanout = 5) at a frequency of 250 Hz (*18*). Further improvements are expected from increasing polymer mobility and PEDOT conductivity, and reducing channel length and source-drain-to-gate overlap capacitance ($C_{sd\text{-}g} \approx 5$ pF for $W = 2000$ μm).

The performance of our inkjet-printed, all-polymer TFT circuits is believed to be adequate for applications such as active-matrix displays or identification tags. The TFT performance and the inverter switching speed are comparable to that of all-polymer TFT circuits reported by the Philips group who used a three-level photolithographic process to pattern electrodes and via-holes (*4, 19*). We believe that our IJP process will allow a similar degree of circuit complexity. IJP has advantageous attributes that will be required for continuous reel-to-reel processing of large-area circuits on plastic substrates. Because only a hydrophobic/hydrophilic surface energy contrast but no topographic profile is required for ink confinement, the photolithographic substrate prepatterning using polyimide can easily be replaced by soft lithography or photopatterning of a self-assembled monolayer (*20*), so that the entire circuit fabrication, including via-hole interconnections consists only of successive solution coating and printing steps. Particular advantages of IJP are as follows: (i) Different materials can be delivered simultaneously from multiple nozzles. (ii) IJP provides accurate registration over large areas, because the inkjet head can be aligned locally with respect to a previously deposited pattern. The local registration, which can be automated, is particularly important for flexible substrates, which inevitably exhibit distortions. (iii) Application- or even end-user–specific circuits can be defined by simple IJP of a network of interconnections and via-holes on a prefabricated array of transistor gates.

The physical mechanism underlying the precise self-alignment of inkjet-printed electrodes with the hydrophobic confinement structure is complex. It involves the simultaneous dynamic processes of droplet spreading and solidification, resulting in an increase of viscosity in the advancing front of the droplet (*21*). Our dynamic, nonequilibrium droplet deposition technique overcomes inherent problems associated with forming high-resolution features by liquid-phase deposition onto patterned substrates. In static equilibrium, liquid patterns suffer from problems such as bulge formation (*22*), capillary breakup, or a sensitive dependence of film thickness on the shape and size of the pattern (*23*). None of these problems occurred in the IJP process, which allows precise local control of deposited droplet volume and drying time to form patterns with arbitrary shape and thickness. The submicrometer precise alignment observed in AFM topographs (Fig. 1A) suggests that our process can be extended to definition of even finer, possibly submicrometer features.

References

1. H. E. Katz *et al*., *Nature* **404**, 478 (2000).
2. H. Sirringhaus *et al*., *Nature* **401**, 685 (1999).
3. R. F. Service, *Science* **278**, 383 (1997); F. Garnier, R. Hajlaoui, A. Yassar, P. Srivastava, *Science* **265**, 1684 (1994).
4. C. J. Drury, C. M. J. Mutsaers, C. M. Hart, M. Matters, D. M. de Leeuw, *Appl. Phys. Lett.* **73**, 108 (1998).
5. J. A. Rogers, Z. Bao, A. Makhija, P. Braun, *Adv. Mater.* **11**, 741 (1999).
6. H. Sirringhaus, N. Tessler, R. H. Friend, *Science* **280**, 1741 (1998).
7. T. R. Hebner, C. C. Wu, D. Marcy, M. H. Lu, J. C. Sturm, *Appl. Phys. Lett.* **72**, 519 (1998).
8. Y. Yang, S.-C. Chang, J. Bharathan, J. Liu, *J. Mater. Sci.: Mater. Electron.* **11**, 89 (2000).
9. T. Shimoda *et al*., *Proc. Soc. Inf. Disp.* **99**, 376 (1999).
10. H. Sirringhaus *et al*., *Appl. Phys. Lett.* **77**, 406 (2000).
11. Z. Bao, Y. Feng, A. Dodabalapur, V. R. Raju, A. J. Lovinger, *Chem. Mater.* **9**, 1299 (1997).
12. W. S. Beh, I. T. Kim, D. Qin, Y. Xia, G. M. Whitesides, *Adv. Mat.* **11**, 1038 (1999).
13. J. A. Rogers, Z. Bao, V. R. Raju, *Appl. Phys. Lett.* **72**, 2716 (1998).
14. S. Jain, *Solid State Electron.* **32**, 77 (1989).
15. S. Luan, G. W. Neudeck, *J. Appl. Phys.* **72**, 766 (1992).
16. T. M. Brown *et al*., *Appl. Phys. Lett.* **75**, 1679 (1999).
17. A. J. Campbell *et al*., *Appl. Phys. Lett.* **76**, 1734 (2000).
18. T. A. de Massa, Z. Ciccone, *Digital Integrated Circuits* (Wiley, New York, 1996).
19. G. H. Gelinck, T. C. T. Geuns, D. M. de Leeuw, *Appl. Phys. Lett.* **77**, 1487 (2000).
20. H. Sugimura, K. Ushiyama, A. Hozumi, O. Takai, *Langmuir* **16**, 885 (2000).
21. P. G. de Gennes in *Liquids at Interfaces*, J. Charvolin *et al*., Eds. (Elsevier Science, Amsterdam, 1989), vol. 48, pp. 273–291.
22. H. Gau, S. Herminghaus, P. Lenz, R. Lipowsky, *Science* **283**, 46 (1999).
23. A. Darhuber, S. M. Troian, S. Miller, S. Wagner, *J. Appl. Phys.* **87**, 7768 (2000).

13 September 2000; accepted 6 November 2000

Ultrahigh-Density Nanowire Arrays Grown in Self-Assembled Diblock Copolymer Templates

T. Thurn-Albrecht,[1] J. Schotter,[2] G. A. Kästle,[2] N. Emley,[2] T. Shibauchi,[3,4] L. Krusin-Elbaum,[3] K. Guarini,[3] C. T. Black,[3] M. T. Tuominen,[2]* T. P. Russell[1]*

We show a simple, robust, chemical route to the fabrication of ultrahigh-density arrays of nanopores with high aspect ratios using the equilibrium self-assembled morphology of asymmetric diblock copolymers. The dimensions and lateral density of the array are determined by segmental interactions and the copolymer molecular weight. Through direct current electrodeposition, we fabricated vertical arrays of nanowires with densities in excess of 1.9×10^{11} wires per square centimeter. We found markedly enhanced coercivities with ferromagnetic cobalt nanowires that point toward a route to ultrahigh-density storage media. The copolymer approach described is practical, parallel, compatible with current lithographic processes, and amenable to multilayered device fabrication.

Continued advances in technologies such as magnetic storage and optoelectronics depend crucially on the ability to produce ultrahigh-density arrays of nanometer-scale elements (*1–11*). As critical device dimensions shrink to the nanometer scale, the parallel fabrication of well-ordered arrays becomes increasingly difficult. We demonstrate a method to rapidly and reliably fabricate arrays with densities in excess of 1 terabit per square inch, based on the self-assembled morphology in diblock copolymer thin films. An ordered, nanoporous structure obtained from the copolymer film by chemical modification is

[1]Polymer Science and Engineering Department, [2]Physics Department, University of Massachusetts, Amherst, MA 01003, USA. [3]IBM T. J. Watson Research Center, Yorktown Heights, NY 10598, USA. [4]Los Alamos National Laboratory, Los Alamos, NM 87545, USA.

*To whom correspondence should be addressed. E-mail: tuominen@physics.umass.edu (M.T.T.); russell@mail.pse.umass.edu (T.P.R.)

used as a template for dc electrodeposition. The result is a highly ordered organic-inorganic hybrid structure. As an example, we fabricate well-ordered, vertical arrays of ferromagnetic nanowires with aspect ratios that are tunable over a wide range. These dense magnetic arrays show enhanced coercivity that points toward a route to ultrahigh-density magnetic storage media.

Electrodeposition in porous materials has been used previously to produce nanowire arrays, in most cases, based either on track-etched membranes or anodized aluminum (*12*, *13*). In comparison to the block copolymer templates introduced here, track-etched membranes have a considerably lower pore density, and the pores are randomly positioned and much less parallel. Porous anodized aluminum templates can achieve lateral densities (*14*, *15*) comparable to that achieved by a block copolymer template, although the production of well-ordered arrays requires special etching procedures (*16*, *17*) or prepatterned samples (*18*). The preparation of the copolymer templates avoids the strong acid etching conditions necessary for anodizing aluminum and enables a new pathway to the fabrication of nanowire templates. We note the flexibility of the block copolymer approach, whereby the nanoscale template can be prepared on any conducting substrate. In contrast to anodized aluminum, there is no insulating barrier layer at the bottom of the nanopores, such that direct dc electrical contact to the substrate is possible. The copolymer-template approach is also based on well-ordered equilibrium structures, which can be controlled by the macromolecular architecture, scaled by the molecular weight, and generalized to other block copolymer microstructures. Because the process is chemical in nature, this route is simple, parallel, compatible with current lithographic processes, and amenable to multilayered device fabrication.

We produced the templates for nanowire arrays using diblock copolymers composed of polystyrene and polymethylmethacrylate, denoted P(S-b-MMA), with a molecular weight of 39,600 daltons and a polydispersity 1.08. The volume fraction of styrene was 0.71, so that in the bulk, the copolymer self-assembles into arrays of 14-nm-diameter PMMA cylinders hexagonally packed in a PS matrix with a lattice constant of 24 nm. Diblock copolymer films (~1 μm thick) were spin-cast from toluene solutions onto a conducting substrate (silicon, gold-coated silicon, or aluminized Kapton). Annealing the diblock copolymer film for 14 hours at 165°C, above the glass transition temperature of both components (105°C for PS and 115°C for PMMA) under an applied electric field (Fig. 1A), causes the cylindrical microdomains to orient parallel to the field lines (*19*–*23*). The dc field (30 to 40 V/μm) was applied across the bottom gold electrode and a second aluminized Kapton film placed on top of the copolymer. The sample was cooled to room temperature before the field was removed, and the upper electrode was peeled away. Deep ultraviolet exposure (25 J/cm^2 dosage) degrades the PMMA domains and simultaneously cross-links the PS matrix such that the degraded PMMA can be removed by rinsing with acetic acid. The resulting nanoporous PS film is optically transparent and contains 14-nm-diameter pores (*21*) that span the film thickness. Electrodeposition (*24*–*26*) is an efficient way to fill the large–aspect ratio nanopores with continuous metal nanowires. Co and Cu nanowire arrays were prepared, demonstrating the generality of our process. Here, we focus on Co (*27*), a relevant material for high-density, magnetic nanowire arrays.

The initial copolymer morphology must be retained throughout the entire fabrication process. Small-angle x-ray scattering (SAXS) was used as a nondestructive means of studying the internal structure of the film. The absolute scattering cross section per unit volume, $d\Sigma/d\Omega$, is given by the product of a contrast factor K and an interference function $S(q)$:

$$\frac{d\Sigma}{d\Omega} = KS(q)$$

where $K = r_e^2\Delta\rho_e^2$, r_e is classical electron radius (2.81×10^{-15} m), and $\Delta\rho_e^2$ is the square of the electron density difference between the two phases. $S(q)$, dictated by the shape and spatial arrangement of the phases (an ordered array of hexagonally packed cylinders), determines the angular dependence of the scattering. Thus, any change in this structure can be easily observed (*28*). The replacement of PMMA in the block copolymer with air ($\rho_e \approx 0$) and then with Co causes marked changes in the contrast and, therefore, the intensity of scattering.

The orientation-dependent polarization energy associated with the cylinders, dielectric bodies that are anisotropic in shape, will align the cylinders parallel to the electric field lines (*19*–*23*). Under strong enough fields, interfacial interactions can be overcome to produce cylindrical microdomains oriented normal to the substrate (*20*, *21*). Viewed from the side, a hexagonally packed array of cylinders oriented normal to the substrate is laterally periodic. Thus, the scattering pattern measured at a finite incidence angle consists of two equatorial Bragg peaks. Figure 2A shows the scattering pattern for an oriented array of the P(S-b-MMA). Two reflections on the equator are evident. Because the sample is only 1 μm thick and the electron densities of PS and PMMA are similar, the reflections are weak. In Fig. 2B, a scattering pattern from the same film is shown after removal of the PMMA cylinders. The intensity of the equatorial peaks has increased by a factor of 54, which is in quantitative agreement with calculations assuming complete removal of the PMMA. Also, the peak position has remained unchanged, showing that the structure has not been altered.

Each 14-nm-diameter pore is essentially a nanoelectrode with ions diffusing down to the electrode surface along its length. Because of the high pore density, the ion-diffusion-layer patterns feeding each pore are in the "total-overlap" electrochemical response limit (*29*). Thus, this situation is electrochemically identical to that of a planar electrode with the added resistance due to the diffusion of ions down the pore. We found the nanoporous templates to be hydrophobic, because electrodeposition did not occur with pure aqueous plating baths. When we used methanol as a surfactant, the plating solution wet the nanopores (*30*), as verified by SAXS. Figure 2C shows the SAXS pattern obtained after placing a droplet of a methanol-water mixture (20/80) on the sample (covered by a thin mica sheet to prevent evaporation). From the electron densities, the SAXS should decrease by a factor of 240. As seen, the

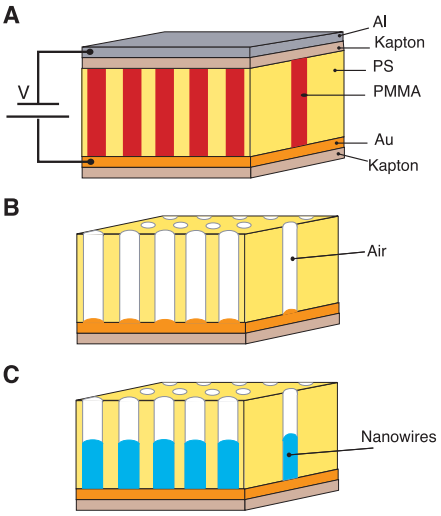

Fig. 1. A schematic representation of high-density nanowire fabrication in a polymer matrix. (**A**) An asymmetric diblock copolymer annealed above the glass transition temperature of the copolymer between two electrodes under an applied electric field, forming a hexagonal array of cylinders oriented normal to the film surface. (**B**) After removal of the minor component, a nanoporous film is formed. (**C**) By electrodeposition, nanowires can be grown in the porous template, forming an array of nanowires in a polymer matrix.

scattering has essentially vanished. Upon drying, the two original peaks appear again. When pure water was used, where the contrast matching should be even better, the SAXS (Fig. 2D) was essentially the same as the dry array (Fig. 2B), showing that water did not penetrate into the pores.

The electroplating process produces a homogeneous Co array that is optically black, as would be expected for a particulated metal film of closely spaced nanoscale cylinders (*31*). Scattering patterns from the templated film before and after plating are shown in Fig. 2, E and F. A strong increase in scattering was observed. Replacing air in the pores with Co should increase the intensity by a factor of 39. The measured intensity increased by only half this value, because the pores were approximately half-filled (500 nm height). Indeed, the intensity of the scattering provided a simple measure of the length of the Co wires deposited in the pores. These results also show that we can control the height or length of the nanowire in the pores while maintaining a constant areal density. In magnetic data storage, for example, large aspect ratio elements are needed to prevent the onset of superparamagnetism (*32*). SAXS measurements also show that the original copolymer morphology is retained throughout the entire fabrication process, leading to an ordered array of Co cylinders with a density of 1.93×10^{11} cylinders per cm^2 (1.25×10^{12}/$inch^2$).

Scanning electron microscopy (SEM) confirms that the electrodeposit nucleates in each pore independently. An SEM image (using the secondary electron signal) of a cross-sectional fracture surface of the Co nanowire array (Fig. 3) that cuts across several layers of the nanowire array corresponds to the schematic in Fig. 1C. The array, composed of 14-nm wires, is evident. The length of the wires is ~500 nm, in agreement with the SAXS measurements. The small length variations indicate that the electrodeposition of the wires occurred uniformly across the template and that the wire diameters are uniform. The total thickness of the template was 1 μm, as indicated by the change in contrast at the surface. Although the contrast is poor, the SEM image indicates the presence of the nanopores above the nanowires into which the nanowires were growing.

The magnetization properties of an array of 14-nm-diameter Co nanowires with an aspect ratio of 36 are shown in Fig. 4. A salient feature in the data is the notably large coercivity field H_c (3000 Oe at 5 K and 800 Oe at 300 K) for field direction parallel to the wire axis (perpendicular to substrate). This large H_c is compared with the behavior of the continuous Co film also shown, which has a coercivity on the order of 10 Oe, considerably smaller than the theoretical anisotropy field (*33*) of ~7000 Oe, due to the easy nucleation and propagation of magnetic domain walls (*32*). In the arrays examined here, the wire diameter is considerably smaller than the theoretical critical single-domain diameter (~50 nm), such that single-domain behavior is possible. Consistent with large aspect ratio and short interwire distance, both the coercive and the saturation fields are higher for the magnetic field applied along the wires than in the transverse direction (perpendicular to the wires). In such a high-density array, there are strong dipolar interactions that present an effective mean field $H_{dipolar} \propto L/s^3$, where L is the length of wires and s is the distance between them (*34*). In the longitudinal-field configuration, while the shape anisotropy acts to align magnetic moments of wires in the same direction, the dipolar interactions favor the pseudo-antiferromagnetic alignment, so that the effective field acting on each nanowire is reduced by $H_{dipolar}$. In the transverse configuration, the field acting on each nanowire is the sum of applied and dipolar fields of the same sign (*5*), and an opposing demagnetizing field due to extreme shape

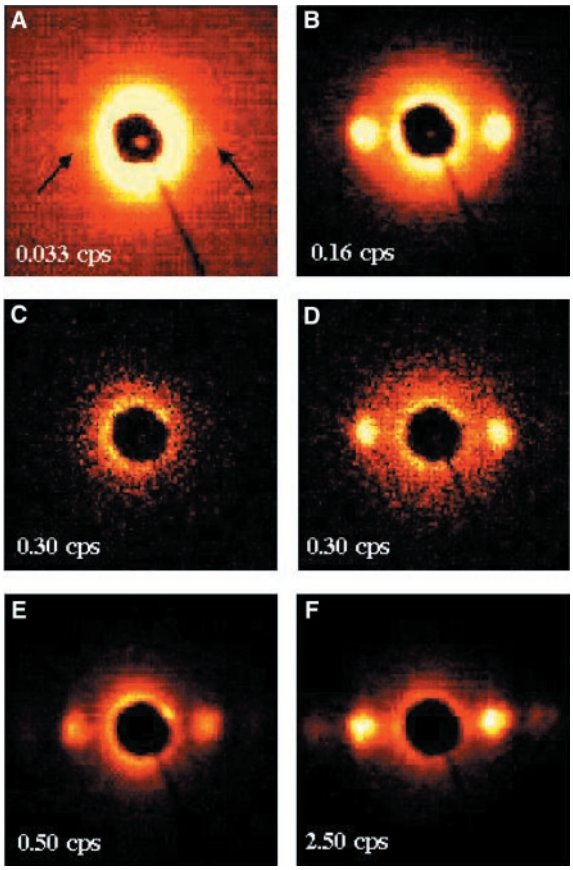

Fig. 2. Small-angle x-ray scattering patterns taken at different steps during the process of nanowire fabrication. All measurements were made at an angle of incidence at 45°. (**A**) Sample oriented in the electric field. Two weak equatorial reflections (indicated by arrows) show the alignment of the cylindrical microdomains oriented in the electric field normal to the surface. (**B**) Because of the increased contrast after pore formation the scattering intensity is strongly enhanced, whereas the position of the peaks is unchanged. (**C**) A water-methanol mixture wets the interior of the pores; because of contrast matching, the scattering pattern disappears. (**D**) Water alone does not wet the interior of the pores; the scattering pattern remains unchanged. (**E** and **F**) Scattering pattern obtained from the same sample before (E) and after (F) electroplating with Co. Because of the high electron density of Co the intensity increases strongly. Again, the peak positions remain unchanged. Higher order reflections can be seen, indicating the highly ordered structure of the nanowire array. Note that the difference between (B) and (E) arises from the change in scale.

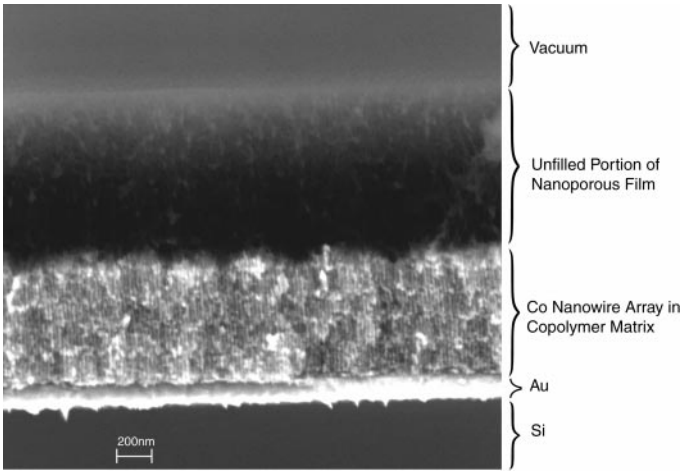

Fig. 3. SEM image of a fracture surface of an array of Co nanowires grown within an array of nanopores formed from block copolymers. The growth of the nanowires was terminated before the template was completely filled, and above the nanowires of Co is the unfilled array of nanopores.

elongation. Thus, the effective field is larger in the transverse case, which is why there is an apparent higher saturation field for the field applied along the nanowires. This outcome is a result of the competition between the dipolar and demagnetizing fields and can be controlled by adjusting the length of the wires and/or interwire distance.

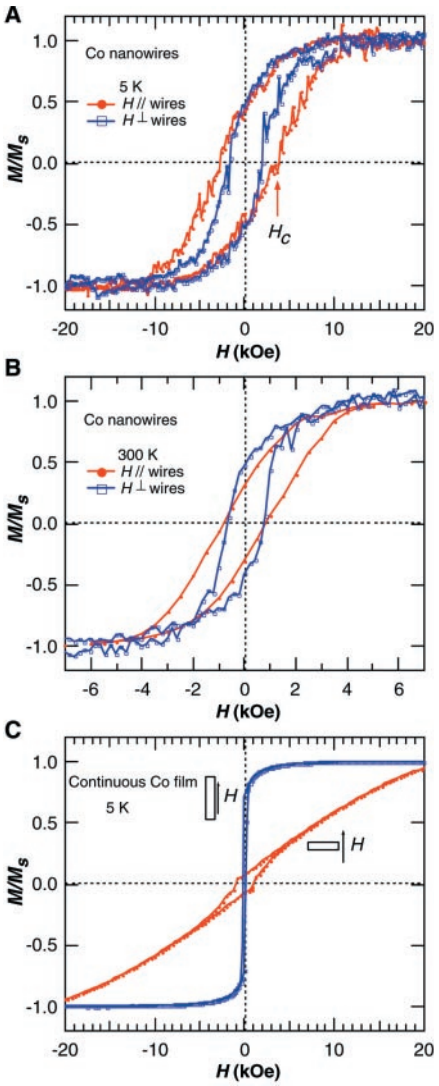

Fig. 4. Magnetic response of Co nanowires. (**A**) Magnetic hysteresis at $T = 5$ K of an array of Co nanowires with diameters of 14 nm, wire lengths of 500 nm, and array period of 24 nm. Curves for the field both parallel to and perpendicular to the wire axis are shown. Each curve was normalized to full saturation. The large coercive field is a substantial fraction of the anisotropy field value for Co (~7000 G). (**B**) Hysteresis data on the same sample at 300 K. (**C**) Magnetic hysteresis loops of a continuous Co film shown for comparison have considerably smaller coercivity. The electrochemically grown film is 500 nm thick. The small square loop near the origin for the perpendicular orientation originates from a configurational reorientation of the in-plane magnetic domains. Measurements were performed with a Quantum Design MPMS superconducting quantum interference device magnetometer.

The regularity of the array is essential here. In ultrahigh-density recording, it minimizes the so-called media noise, i.e., accidental switching of bits due to the distribution of the coercive and saturation fields (*32*, *35*). When the distance s between the nanowires is highly distributed due to disorder, $H_{dipolar}$ is locally enhanced, inducing easy nucleation and propagation of domains encompassing a number of wires, and hence reducing coercivity. Coercivity enhancements may also be reduced by a larger effective diameter of the overlapping nanowires inherent, for example, in the track-etching techniques (*25*, *36*). An ordered array having a sufficiently large coercivity represents a route to single-domain, ultrahigh-density magnetic data storage media, while at the same time permitting sufficiently large aspect ratio magnetic nanowires to circumvent the detrimental effects of superparamagnetism (*37*). The fabrication process can be easily fine-tuned to optimize properties for media applications by changing the aspect ratio and separation distance of the wires.

Although we have focused on the generation of arrays of magnetic nanowires, the potential impact of the copolymer templates is much broader. By means of the identical procedures outlined here, thermoelectric cooling devices (*9*) with controlled nanowire diameters can easily be fabricated. The ordered array of nanopores can also be used as templates to transfer the copolymer structure into the substrate (*3*). In addition, the nanopores can be used as nanoreactors where catalysts can be anchored to the base of the pores or simply as a scaffold in which silicon oxide can be grown. Finally, an electron beam can be used to place the nanopores at specific positions on the sample, affording a means of controlling the lateral placement of nanostructures on a surface. Consequently, controlling the orientation of copolymer morphologies in thin films offers a very practical means of producing nanostructures that are amenable to technological applications.

References and Notes

1. J. Wong, A. Scherer, M. Todorovic, S. Schultz, *J. Appl. Phys.* **85**, 5489 (1999).
2. S.-Y. Chou, *Proc. IEEE* **85**, 652 (1997).
3. M. Park, C. Harrrison, P. M. Chaikin, R. A. Register, D. H. Adamson, *Science* **276**, 1401 (1997).
4. S. Wirth, S. V. Molnar, M. Field, D. D. Awscholom, *J. Appl. Phys.* **85**, 5249 (1999).
5. G. J. Strikjers, J. H. J. Dalderop, M. A. A. Broeksteeg, J. J. M. Swagten, W. J. M. de Jonge, *J. Appl. Phys.* **86**, 5141 (1999).
6. J. M. Garcia *et al.*, *J. Appl. Phys.* **85**, 5480 (1999).
7. T. L. Hylton *et al.*, *Appl. Phys. Lett.* **67**, 1154 (1995).
8. S. Fan *et al.*, *Science* **283**, 512 (1999).
9. J. Heremans, C. M. Thrush, *Phys. Rev. B* **59**, 12579 (1999).
10. G. Fasol, *Science* **275**, 941 (1999).
11. J. Chen, M. A. Reed, A. M. Rawlett, J. M. Tour, *Science* **286**, 1550 (1999).
12. J. C. Hulteen, C. R. Martin, *J. Mater. Chem.* **7**, 1075 (1997).
13. A. Huczko, *Appl. Phys. A Mater. Sci. Proc.* **70**, 365 (2000).
14. D. Routkevitch, T. Bigioni, M. Moskovits, J. M. Xu, *J. Phys. Chem.* **100**, 14037 (1996).
15. H. Zeng *et al.*, *J. Appl. Phys.* **87**, 4718 (2000).
16. H. Masuda, K. Fukuda, *Science* **268**, 1466 (1995).
17. A. P. Li, F. Müller, A. Birner, K. Nielsch, U. Gösele, *J. Appl. Phys.* **84**, 6023 (1998); *Adv. Mater.* **11**, 483 (1999).
18. H. Masuda, H. Yamada, M. Satoh, H. Asoh, *Appl. Phys. Lett.* **71**, 2770 (1997).
19. T. L. Morkved *et al.*, *Science* **273**, 931 (1996).
20. T. Thurn-Albrecht, J. DeRouchey, T. P. Russell, H. M. Jaeger, *Macromolecules* **33**, 3250 (2000).
21. T. Thurn-Albrecht *et al.*, *Adv. Mater.* **12**, 787 (2000).
22. K. Amundson, E. Helfand, X. Quan, S. D. Smith, *Macromolecules* **26**, 2698 (1993).
23. K. Amundson, E. Helfand, X. Quan, S. D. Hudson, S. D. Smith, *Macromolecules* **27**, 6559 (1994).
24. S. Kawai, *Symposium on Electrochemical Technology in Electronics* (Electrochemical Society, Pennington, NJ, 1987).
25. T. M. Whitney, J. S. Jiang, P. C. Searson, C. L. Chien, *Science* **261**, 1316 (1993).
26. P. V. Braun, P. W. Wiltzius, *Nature* **402**, 603 (1999).
27. The room-temperature electrolyte bath contained 20% by volume methanol, Co salt (1.3 M $CoSO_4 \cdot 5H_2O$), and a buffering acid (0.7 M H_3BO_3) at a pH of 3.7, prefiltered through a 0.2-μm filter. A standard three-electrode cell configuration (*38*) was used with a computer-controlled, galvanostatic (constant current) electroplating circuit. The exposed gold on the template sample forms the working electrode, and its half-cell potential is monitored with respect to a standard calomel reference electrode (SCE). The counterelectrode is a platinum foil with an 8-cm^2 surface area. A potential at least as negative as −0.52 V (the half-cell electrode potential against the SCE for $Co^{2+} + 2e^- \rightarrow Co$) must be applied by the biasing circuit. Electrodeposition begins at the exposed gold at the base of each nanopore and grows upward as the pore is filled. Electrodeposition ensures continuity of the nanowire wires, because otherwise growth cannot be sustained. Constant-current densities of 30 to 300 A/m^2 resulted in deposition rates of 1 to 10 nm/s. We controlled nanowire height by monitoring the integrated current.
28. SAXS experiments were performed with Ni-filtered Cu-Kα radiation from a Rigaku rotating anode operated at 8 kW with pinhole collimation at an angle of incidence of 45°. The scattering was recorded on a gas-filled area detector (Siemens Hi-Star). The electron densities (in $e^-/Å^3$) are given in parentheses for PS (0.341), PMMA (0.386), water (0.335), water-methanol (0.319), and Co (2.456).
29. J. C. Hulteen, V. P. Menon, C. R. Martin, *J. Chem. Soc. Faraday Trans.* **92**, 4029 (1996).
30. See, for example, the discussion of LIGA in M. Madou, *Fundamentals of Microfabrication* (CRC Press, Boca Raton, FL, 1997).
31. C. A. Foss, G. L. Hornyak, J. A. Stockert, C. P. Martin, *J. Phys. Chem.* **98**, 2963 (1994).
32. D. Weller, A. Moser, *IEEE Trans. Magn.* **35**, 4423 (1999).
33. G. Bertotti, *Hysteresis in Magnetism* (Academic Press, New York, 1998).
34. J. Garcia-Otera, M. Porto, J. Rivas, A. Bunde, *Phys. Rev. Lett.* **84**, 167 (2000).
35. M. Hehn *et al.*, *Science* **272**, 1782 (1996).
36. L. Sun, D. C. Searson, C. L. Chien, *J. Appl. Phys.* **74**, 2803 (1999).
37. O. Fruchart, M. Klaua, J. Barthel, J. Kirschner, *Phys. Rev. Lett.* **83**, 2769 (1999).
38. A. J. Bard, L. R. Faulkner, *Electrochemical Methods* (Wiley, New York, 1980).

39. We are grateful to A. Fadeev for helpful discussions concerning the choice of a suitable surfactant and C. Stafford for the preparation of the block copolymer. T.T.-A. acknowledges support by the Deutsche Forschungsgemeinschaft. Funded by the National Science Foundation "Partnership in Nanotechnology" grant, the Materials Research Science and Engineering Center, and the U.S. Department of Energy.

22 August 2000; accepted 9 November 2000